Ar adsorptions on Al (111) and Ir (111) surfaces: a first-principles study*

Niu Wen-Xia(牛纹霞)[a] and Zhang Hong(张 红)[b]†

[a] *Institution of Atomic and Molecular Physics, Sichuan University, Chengdu* 610065, *China*
[b] *College of Physical Science and Technology, Sichuan University, Chengdu* 610065, *China*

(Received 1 June 2011; revised manuscript received 13 July 2011)

We investigate the adsorptions of Ar on Al (111) and Ir (111) surfaces at the four high symmetry sites, i.e., top, bridge, fcc- and hcp-hollow sites at the coverage of 0.25 monolayer (ML) using the density functional theory within the generalized gradient approximation of Perdew, Burke and Ernzerhof functions. The geometric structures, the binding energies, the electronic properties of argon atoms adsorbed on Al (111) and Ir (111) surfaces, the difference in electron density between on the Al (111) surface and on the Ir (111) surface and the total density of states are calculated. Our studies indicate that the most stable adsorption site of Ar on the Al (111) surface is found to be the fcc-hollow site for the (2×2) structure. The corresponding binding energy of an argon atom at this site is 0.538 eV/Ar atom at a coverage of 0.25 ML. For the Ar adsorption on Ir (111) surface at the same coverage, the most favourable site is the hcp-hollow site, with a corresponding binding energy of 0.493 eV. The total density of states (TDOS) is analysed for Ar adsorption on Al (111) surface and it is concluded that the adsorption behaviour is dominated by the interaction between 3s, 3p orbits of Ar atom and the 3p orbit of the base Al metal and the formation of sp hybrid orbital. For Ar adsorption on Ir (111) surface, the conclusion is that the main interaction in the process of Ar adsorption on Ir (111) surface comes from the 3s and 3p orbits of argon atom and 5d orbit of Ir atom.

Keywords: density-functional theory, binding energy, adsorption, electronic structure

PACS: 68.43.–h, 68.43.Fg, 68.47.De **DOI:** 10.1088/1674-1056/21/2/026802

1. Introduction

Aluminum is one of the most metal storages in the world. Aluminum powder is the most commonly used as metallic additive in explosives, propellants and pyrotechnic in order to improve the performances of high energetic materials.[1] The aluminum is utilized to augment the energy to the burning effect and raise the flame temperature in rocket propellants and is used to enhance the blast-effect of explosives and improve the performance underwater.[1–4] Al nanoparticle can promote chemical reactions for its large surface area, small size (the particle size was between 100 nm–200 nm) and lots of other performances. Additon of Al nanopowder into propellants can improve the burning performance and enhance the burning ratio. Some researchers have reported that addition of Al nanoparticle into explosion can strengthen explode properties.[2–8]

The study on the application of aluminum nanoparticle has made certain progress in solid propellants and found that addition of aluminum nanoparticle (Alex)[5] into solid propellants results in an increase in the burn rate. But an important issue, particularly for nanoscale Al powder, is that aluminum is a highly reactive metal and interacts with oxygen easily in the air, leading to the generation of a pre-pressing and solid oxide overcoat before its burning, which inhibits the efficient burning and severely reduces the utilization rate of aluminum. Gao[9] reported that the combustion ratio of aluminum nanoparticle increases nearly two orders of magnitude than that of normal aluminum, so it was coated using the inert materials in order to maintain its performances. Because of its notable inertness, argon gas is considered to serve as a shielding gas in aircraft manufacturing, shipbuilding, atomic energy industry and machinery industry. In metal smelting and electronic industry, argon gas always plays a protective role.

Because iridium-based alloys can form an effective antioxidizing diffusion barrier, they are important for developing ultrahigh-temperature oxidation-

*Project supported by the National Natural Science Foundation of China (Grant No. 11074176 and 10976019) and the Doctoral Program of Higher Education of China (Grant No. 20100181110080).

†Corresponding author. E-mail: hongzhang@scu.edu.cn

© 2012 Chinese Physical Society and IOP Publishing Ltd

resistant coatings.[10,11] In order to avoid the formation of the toxic gaseous oxide, IrO_3, iridium always alloyed with aluminum.[12] In this paper, we present a detailed study of using rare-gas to protect it, for rare-gas atom has closed shells (spherical symmetry), the simple electronic structure and the weak interaction with surfaces. Chemical reactions easily take place on Al (111) and Ir (111) surfaces, so those topics are very hot for chemical model investigations for the researchers. In the present paper, we begin with studying the inert material argon adsorptions on Al (111) and Ir (111) surfaces. As is well known, there are no experimental or first-principles studies of those systems and there is little theoretical work on the study of the electronic properties of argon adsorption on Al (111) and Ir (111) surfaces. Hence, these topics are necessary to understand first the atomic and the electronic structures of the Ar/Al and Ar/Ir alloys. The remainder of the present paper is organized as follows. In Section 2, a brief description of our computational method is given and parameters settings are listed. In Section 3, the results and the discussions are presented. Finally the conclusions are dawn from the present study in Section 4.

2. Calculation method

In this paper all the calculations are performed in the framework of the density functional theory (DFT),[13,14] as implemented in the CASTEP[15] package, where we employ the generalized-gradient approximation (GGA) of Perdew, Burke and Ernzerhof (PBE)[16] for the exchange–correlation functional. Ultrasoft pseudopotentials[17] are used for all calculations. The Al (111) and the Ir (111) surfaces are modeled in the supercell slab approach, where five layer Al (111) and Ir (111) slabs with a vacuum region of 12 Å (1 Å = 0.1 nm) and (2×2) structure of all calculations are used and the periodic supercell contains 20 metal atoms in the five-layer slab of Al and Ir. The argon atom is adsorbed on one side of the slab only at a quarter monolayer coverage (0.25 ML).

In our calculations, Ar atoms are adsorbed on Al (111) and Ir (111) at the four high symmetry sites: the top, bridge, fcc-hollow and hcp-hollow sites. The positions of atoms in the two topmost Al (111) and Ir (111) layers and the argon atoms in on-surface sites are allowed to fully relax and the atomic coordinates of the remaining three metal layers are fixed. For the surface calculations, the wave functions are expanded in a plane-wave basis set with an energy cutoff of 300 eV. The convergence criterion for the total energy, force on the atoms and displacements are set to be 2×10^{-5} eV, 5×10^{-1} eV/nm and 2×10^{-4} nm. The Brillouin-zone integration is performed using $(4 \times 4 \times 1)$ Monkhorst–Pack (MP) grid of k-points for the (2×2) surface unit cell. The effects of the spin polarization for the systems are so small that in our calculations they can be ignored.[18] Convergence tests indicate that these settings are sufficient to achieve a high accuracy by changing the k-points and the cutoff energy.

The stability of Ar/metal structure with respect to adsorption of Ar is obtained by calculating the average binding energy per Ar adatom. The average binding energy, $E_{\rm b}^{\rm Ar/metal}$, is defined as[19]

$$E_{\rm b}^{\rm Ar/metal} = -\frac{1}{N_{\rm Ar}}[E^{\rm Ar/metal} - (E^{\rm metal} + N_{\rm Ar}E^{\rm Ar})], \quad (1)$$

where $N_{\rm Ar}$, $E^{\rm Ar/metal}$, $E^{\rm metal}$ and $E^{\rm Ar}$ are the number of Ar atoms per unit cell, the total energies of the adsorbate-ubstrate system, the clean surface and the isolated argon atom respectively. A positive number of the binding energy indicates that the adsorption process is exothermic with respect to the free Ar atom and a negative value shows that the process is endothermic.

An important quantity which helps to characterize the orbitals that are related to the interaction between adsorbate and substrate is the difference in electron density, $n^{\triangle}(r)$, which is calculated as[19]

$$n^{\triangle}(r) = n^{\rm Ar/metal}(r) - n^{\rm metal}(r) - n^{\rm Ar-layer}(r), \quad (2)$$

where $n^{\rm Ar/metal}(r)$ is the total electron density of the Ar/metal system, $n^{\rm metal}(r)$ and $n^{\rm Ar-layer}(r)$ are the total electron densities of the clean surface and the free Ar-layer, respectively.

3. Results and discussion

3.1. Bulk and clean surfaces

Before studying the effects of argon adsorption on Al (111) and Ir (111) surfaces, we first calculate the properties of the bulk metal systems and analyse the metal surface structures in their most stable phases, i.e., the face-centered cubic for Al and Ir. Our calculations show clearly that the bulk lattice constant

of Al is $\alpha_0 = 4.004$ Å with neglecting zero-point vibration. The bulk modulus, $B = 0.700$ Mbar (1 bar $= 10^5$ Pa) and the cohesive energy, $E_{\rm coh} = 4.00$ eV, which are in agreement with the commonly established experimental values $\alpha_0 = 4.05$ Å,[20] $B = 0.720$ Mbar and $E_{\rm coh} = 3.39$ eV.[21] The values are also in-line with other reported results which are listed in Table 1. For Ir bulk the lattice constant is $\alpha_0 = 3.86$ Å with neglecting zero-point vibration, the bulk modulus $B = 3.50$ Mbar and the cohesive energy, $E_{\rm coh}$, is calculated to be 7.16 eV, which are also in reasonable agreement with experimental values $\alpha_0 = 3.84$ Å, $B = 3.55$ Mbar, $E_{\rm coh} = 6.94$ eV,[22] and other calculations are listed in Table 1.

The obtained interlayer relaxations of the clean Al (111) and the Ir (111) surfaces, $\triangle_{ij} = (d_{ij} - d)/d \times 100\%$ between layers i and j with respect to the bulk spacing ($d = 2.334$ Å for Al and $d = 2.224$ Å for Ir), are shown in Table 1 for the two topmost atomic layers. The positive value indicates that atoms stretch outward, on the contrary, the negative value shows that atoms contract inward. The obtained metal interlayer distances are $d_{12} = 2.300$ Å and $d_{23} = 2.307$ Å for the clean Al (111) surface, showing a contraction of 1.46% for d_{12} relative to the Al bulk value and 1.11% for the second interlayer distance. For the second interlayer distances, which are in good agreement with experimental values 2.1% and 0.6%, respectively.[27,28] It indicates that there are certain relaxations on Al (111) and Ir (111) surfaces and the effect of relaxation of surface atom is weakened from the first layer to the third layer.

3.2. Ar adsorption on metal surface

The values of binding energy $E_{\rm b}^{\rm Ar/metal}$ and the geometric parameters of the systems at the four high symmetry sites, with respect to those of the free argon atom, are displayed in Table 2. For fcc (111) structure, the two three-fold sites (fcc and hcp sites), differ in that the fcc site has a substrate atom directly under it in the third layer and the hcp site has a substrate atom directly under it in the second layer.

Table 1. Lattice constants, bulk modulus and relaxations of outermost layers for Al (111) and Ir (111) for 0.25 ML. d_{12} and d_{23} are the first and second metal interlayer spacings, respectively.

Surface		α_0/Å	B/Mbar	$E_{\rm coh}$/eV	d_{12}/Å	d_{23}/Å
Al (111)	Experimental	4.05[a]	0.720[b]	3.39[b]		
	This work	4.00	0.700	4.00	2.300	2.307
	Other calculations	4.04[d]	0.780[d]	3.60[d]		
		4.04[e]	0.705[e]			
Ir (111)	Experimental	3.84[c]	3.55[c]	6.94[c]		
	This work	3.86	3.50	7.16		
	Other calculations	3.85[f]	3.57[f]	7.45[f]	2.168	2.200
		3.89[g]	3.43[g]			

[a]Ref. [20], [b]Ref. [21],[c]Ref. [22], [d]Ref. [23], [e]Ref. [24], [f]Ref. [25], [g]Ref. [26].

Table 2. Calculated binding energies (in eV), relative to those of a free Ar atom and the relevant geometric parameters (in Å) for Ar atomic adsorption at the four high symmetry sites (top, bridge, fcc- and hcp-hollow sites) for 0.25 ML. $d_{\rm Ar-metal}$ is the bond-length between Ar atom and the nearest metal atom. d_{01} is the vertical height of Ar atomic to the topmost metal layer. $\triangle_{12}$ is the change in distance between the first interlayer and the second metal interlayer and $\triangle_{23}$ is the change in distance between the second layer and the third interlayer. (relative bulk spacings $d = 2.334$ Å and $d = 2.224$ Å, respectively).

Surface	Site	$E_{\rm b}$/eV	$d_{\rm Ar-metal}$/Å	d_{01}/Å	$\triangle_{12}$(%)	$\triangle_{23}$(%)
Al (111)	fcc-hollow	–0.538	3.810	3.460	–2.51	–2.39
Al (111)	hcp-hollow	–0.536	3.778	3.457	–2.83	–1.35
Al (111)	bridge	–0.506	3.763	3.512	–2.23	–1.18
Al (111)	top	–0.534	3.444	3.444	–1.89	–1.31
Ir (111)	fcc-hollow	–0.401	3.852	3.530	–2.15	–0.71
Ir (111)	hcp-hollow	–0.493	3.802	3.460	–2.47	–0.58
Ir (111)	bridge	–0.375	3.984	3.739	–2.02	–0.81
Ir (111)	top	–0.393	3.517	3.515	–2.56	–0.58

As shown in Table 2, the more stable sites for Ar adsorption on Al (111) surface are the two three-fold sites, and the fcc-hollow site is energetically most favourable and has a corresponding binding energy of 0.538 eV at 0.25 ML. As is well known, the adsorption for inert gas on surface is weak generally and the binding energy is about 0.434 eV, such as Xe adsorption on Pd (111), which has an adsorption energy range of 0.36 eV–0.33 eV at the high symmetry sites,[29] and Ar adsorption on Pd (111) surface, which has a binding energy of 0.159 eV at the most favourable site (the top site) correspondingly.[29] The results show that this rule is also applicable to the case of Ar atom adsorption on metal surfaces. And the favourable site is consistent with that obtained from the corollary (the on-top site preference for Xe, Kr and He adatoms, but the two three-fold sites for Ne and Ar).[29] Our calculations demonstrate that the binding energies of Ar on Al (111) surface at the fcc- and hcp-hollow sites are similar. For Ar at the hcp-hollow site, the binding energy is just 0.002 eV less favourable than that at the fcc-hollow site. This indicates that the most stable site is the fcc-hollow site of Ar adsorption on Al (111) surface, but the bond length of Ar at the fcc-hollow site is 3.810 Å (as compared with 3.778 Å). From this table, it can be seen that the situation of Ar adsorption on Ir (111) surface is the same as that on Al (111) surface and the two three-fold sites are more stable than the top site and the bridge site. Instead, the more stable site is the hcp-hollow site of Ar adsorption on Ir (111) surface and the corresponding binding energy is 0.493 eV. The next stable site is the fcc-hollow site and the binding energy is 0.401 eV, which is 0.092 eV less favourable than that at the hcp-hollow site. This indicates that the most stable site of Ar adsorption on Ir (111) surface is the hcp-hollow site. The more favourable adsorption site for Ar adsorption on Ir (111) is also reflected by the bond-length of Ar–Ir and the bond-length of Ar at the hcp-hollow site is 3.802 Å (as compared with 3.852 Å). In order to check the effect of the adsorption stability of surface substrate, we need to relax the topmost three metal layers (as compared with two metal layers) and fully relax the Ar atom and we find that the effect on the binding energy is almost negligible.

The calculated atomic geometries of the Ar/metal structure are given in Table 2. Topmost interlayer spacing relaxation with respect to the ideal interlayer surface spacing, is $\Delta_{ij} = (d_{ij} - d)/d \times 100\%$. The positive (negative) sign for the substrate rumpling demonstrates an outward (inward) displacement of the metal atom under the Ar adatom. For argon adsorption on Al (111) at the fcc-hollow site, i.e., the most favourable site, the contractions of the topmost two interlayer spacings are $\Delta_{12} = -2.51\%$ and $\Delta_{23} = -2.39\%$ relative to those of the clean Al (111) surface and a relative bulk spacing is $d = 2.334$ Å. Compared with Ar adsorption on Ir (111) at the most favourable site, i.e., the hcp-hollow site, the contractions of the topmost two interlayer spacings are $\Delta_{12} = -2.51\%$ and $\Delta_{23} = -2.39\%$ relative to those of the clean Ir (111) surface and a relative bulk spacing is $d = 2.224$ Å.

The charge population properties for Ar adsorption on Al (111) and Ir (111) at the two three-fold sites are discussed to further study the electronic structures of the Ar/Al and Ar/Ir systems and the results are detailed in Table 3. The Mulliken charge population analysis is implemented to analyse the charge transfer. It should be pointed out that this method has a certain limitation, so the charge can be considered only in qualitative concept. It can be seen from Table 3 that the values of the charge transfer are positive when Ar adsorptions on Al (111) and Ir (111) surfaces take place at the two hollow sites, which indicates that there is a charge transfer from Ar atoms to the nearest neighbouring metal atoms, i.e., Ar atom behaves as the electron donor and metal atoms as the electron acceptor. From Table 3, it can be seen that no matter whether Ar appears at the fcc-hollow site or hcp-hollow site of Ar/Al system, the charge transfer is unchanged. For Ar on Al (111) at the favourable site (the fcc-hollow site), a charge transfer of 0.01 e occurs from argon atom to the aluminum metal, similar to that when Ar adsorption takes place at the hcp-hollow site. Therefore, we know that the adsorption situations of Ar on Al (111) at the two hollow sites are very close. For Ar/Ir system, the charge transfer is about 0.02 e when Ar adsorption occurs at the hcp-hollow site, a same value of 0.02 e is seen for Ar at the fcc-hollow site. The results show that the adsorption situations of Ar on Ir (111) at the two hollow sites are similar. This indicates that the electron redistributions of Ar on the two metal surfaces are similar to those for Ar at each of the two threefold sites. As is well known, when the electronegativity gradually increases, its ability to attract electron increases gradually. The electronegativity of the Ir atom is 2.20, which is larger than the electronegativity of Al atom, 1.61,[30] so Ir atom can easily obtain electron than Al atom. The results are consistent with our calculations.

Table 3. Mulliken charge populations (in e) of Ar adsorption on metal surfaces at the fcc- and hcp-hollow sites. The argon coverage is 0.25 ML.

Surface	Site	Ar-3s	Ar-3p	Charge
Al (111)	Ar at fcc-hollow site	2.00	5.99	0.01
Al (111)	Ar at hcp-hollow site	2.00	5.99	0.01
Ir (111)	Ar at fcc-hollow site	2.00	5.98	0.02
Ir (111)	Ar at hcp-hollow site	2.00	5.98	0.02

The charge transfer situations of Ar on Al (111) and Ir (111) surfaces at the two threefold sites are also reflected from the difference electron densities (Figs. 1 and 2). The white areas represent charge loss and the black zones denote the charge accumulation. The tangent plane is the (001) plane occupied by the Ar atom and the nearest neighbouring metal atoms. The difference electron density plots have almost the same pattern of redistributions for Ar adsorption on Al (111) and Ir (111) surfaces. The difference electron density of Ar/Al system is shown in Fig. 1 and the difference electron density of Ar/Ir system is exhibited in Fig. 2. It can be seen from Fig. 1 that there are some situations of electronic loss and accumulation around the Al atom. In addition, the charge density distributions of Ar adsorptions on Al (111) surface at the fcc-hollow site and the hcp-hollow site are very similar. These characteristics are also reflected in Table 2. The binding energy of Ar on Al (111) at the hcp-hollow site is just 0.002 eV less favourable than at the

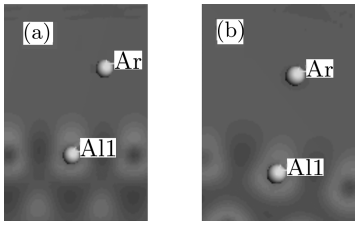


Fig. 1. Difference electron density plots of Ar adsorption on Al (111) at the two threefold sites (0.25 ML). The panel (a) shows Ar at the fcc-hollow site and panel (b) indicates Ar at the hcp-hollow site.

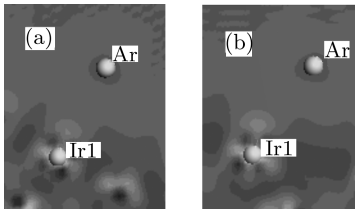


Fig. 2. Difference electron density plots of Ar adsorption on Ir (111) surface at the two three-fold sites (0.25 ML). The panel (a) shows Ar at the fcc-hollow site and panel (b) indicates Ar is at the hcp-hollow site.

fcc-hollow site. For Ar/Ir system, there are also some situations of electronic loss and accumulation around the Ir atom. The difference is that the increase of charge density of Ar at the hcp-hollow site is bigger than at the fcc-hollow site. It indicates that the most favourable site of Ar adsorption on Ir (111) surface is the hcp-hollow site.

In order to gain an insight into the electronic structures of those systems, we consider the total density of states (TDOS) for argon atoms adsorbed on Al (111) and Ir (111) surfaces with 0.25 ML coverage at the four high symmetry sites, which are shown in Figs. 3 and 4 respectively. For comparison, the TDOSs for Al and Ir atoms near the Fermi level in the clean Al (111) and Ir (111) surfaces are presented in Figs. 3 and 4, respectively, where the Fermi level has been set to be zero. From Fig. 3 we can see that it mainly consists of Al (111) 3p orbit. When argon atoms are adsorbed on Al (111) surface, a prominent new peak appears at about 20.5 eV below the Fermi level with 0.25 ML coverage, it is concluded that the contribution belongs to the 3s orbit of Ar atom; meanwhile, the peak at the 6.5 eV below the Fermi level is enhanced, owing to the 3p orbit of Ar atom. It is concluded that the adsorption behaviour is dominated by the interaction between the 3s, 3p orbit of Ar atom and the 3p orbit of the base Al metal. We can see a strang overlap of Al-3p and Ar-3p states at about 5.5 eV below the Fermi level and an effective bonding between Al-3p and Ar-3p states at about 6.5 eV below the Fermi level. However, there is a notable difference between the two three-fold sites of the TDOS, i.e., the Al-3p states for Ar adsorption at the fcc-hollow site (region from –12.0 eV to +3.5 eV) is slightly broader than that at the hcp-hollow site (region from –11.5 eV to +2.5 eV), suggesting a greater hybridization of states for Ar at the fcc-hollow site, which indicates that Ar adsorption at the fcc-hollow site is more stable. The difference in TDOS shows why Ar could be expected to be adsorbed more favourably at the fcc-hollow site. From Fig. 4, we can see that it mainly consists of Ir (111) 5d orbit. When Ar atoms are adsorbed on Ir (111) surface, a prominent new peak appears about 18.5 eV below the Fermi level with 0.25 ML coverage, it is

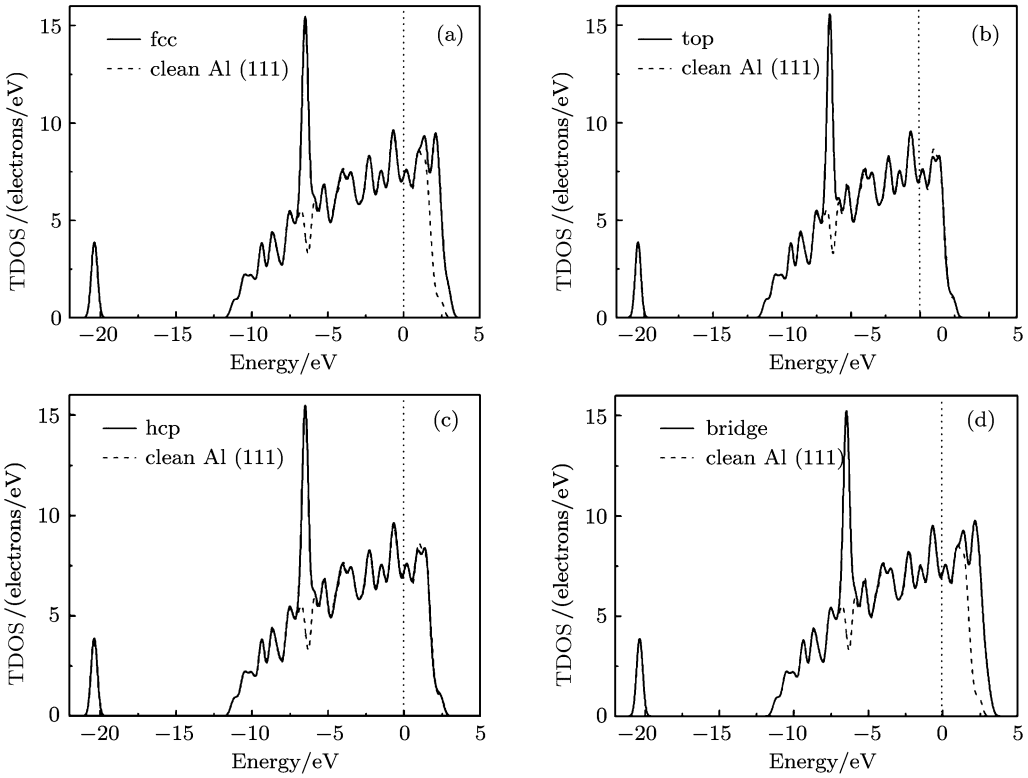


Fig. 3. Total densities of states (TDOSs) for 0.25 ML of argon adsorbed on Al (111) at the four high symmetry sites and the clean Al (111) surface for comparison. The energy reference is the Fermi energy (0 eV).

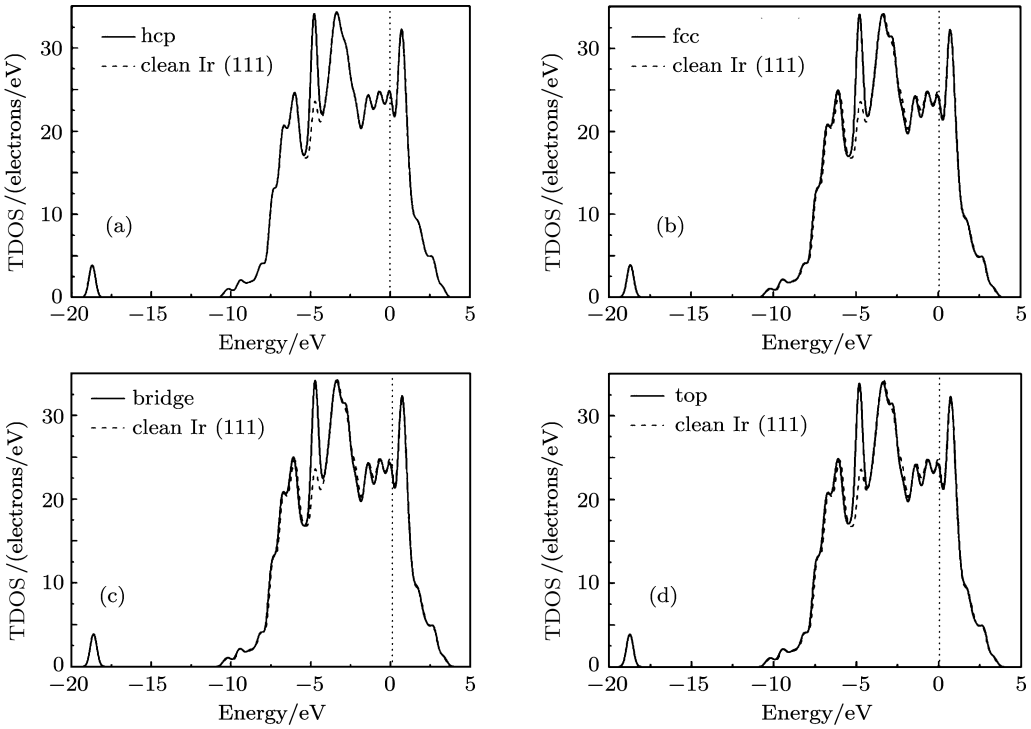


Fig. 4. Total densities of states (TDOSs) for 0.25 ML of argon adsorbed on Ir (111) at the four high symmetry sites and the clean Ir (111) surface for comparison. The energy reference is the Fermi energy (0 eV).

concluded that it is due to the Ar-3s orbit; meanwhile, the peak at the 4.5 eV below the Fermi level is enhanced, which is attributed to the Ar-3p orbit. It indicates that the main interaction in the process of Ar adsorption on Ir (111) surface comes from the 3s, 3p orbits of Ar atom and 5d orbit of Ir atom. Also we can see a strange overlap of Ir-5d and Ar-3p states at about 3.5 eV below the Fermi level and a greater hybridization between Ir-5d and Ar-3p states at about 4.5 eV below the Fermi level. From this figure, we also find that those TDOSs of Ar adsorption at the four high symmetry sites very resemble. There is a minor difference in TDOS between the two threefold sites: the Ir-5d states for Ar adsorption at the hcp-hollow site are higher than at the fcc-hollow site at the Fermi level, which indicates that Ar adsorption at hcp-hollow site is more stable. From that we obtain that Ar adsorptions on Ir (111) surface at the four high symmetry sites are different from Ar adsorptions on Al (111) surface. On Al (111) surface the fcc-hollow site is more stable and on Ir (111) surface the hcp-hollow site is more stable.

From the analyses of the electronic structures of the Ar/Al (111) and Ar/Ir (111) systems, we find that the Ar adsorptions on Al (111) and Ir (111) surfaces at the two threefold sites are more stable than those at the top and bridge sites with 0.25 ML. Difference is that on Al (111) surface the fcc-hollow site is more stable and on Ir (111) surface the hcp-hollow site is more stable.

4. Conclusions

In this paper, the physical and the electronic properties of Ar adsorptions on Al (111) and Ir (111) surfaces at the top, bridge, fcc- and hcp-hollow sites with 0.25 ML are investigated systematically from first principles within the generalized gradient approximation and a supercell approach. It can be seen that Ar adsorptions at the two three-fold sites on those two metal surfaces are more stable than at the top and bridge sites. Our calculations demonstrate that Ar adsorption at the fcc-hollow site on Al (111) is most favourable and the corresponding binding energy is 0.538 eV. For Ar/Ir system, the most stable site of Ar adsorption is Ar at the hcp-hollow site, with a corresponding energy of 0.493 eV. Furthermore, the total densities of states (TDOSs) of Ar atoms adsorptions on Al (111) and Ir (111) surfaces are investigated. The results are due mainly to the interaction between orbits of Ar-3s, 3p and Al-3p orbit when Ar atoms are adsorbed on Al (111) surface and the formation of sp hybrid orbital. The Al-3p states for Ar adsorption at the fcc-hollow site are reflected broader, which shows more effective hybridization of states. It indicates that the Ar adsorption on Al (111) surface at the fcc-hollow site is more favourable. For the Ar on Ir (111) surface, the results are due mainly to the interaction between Ar-3s, 3p orbits and Ir-5d orbit, also we find that the Ir-5d state at the hcp-hollow site is higher than that at the fcc-hollow site at the Fermi level. It indicates that the Ar adsorption on Ir (111) surface at hcp-hollow site is more favourable.

References

[1] Zhou S Q, Zhao F Q, Ju X H, Cheng X C and Yi J H 2010 *J. Phys. Chem.* C **114** 9390

[2] Kuo K K, Brill T B, Resce-Rodriguez R A, Mitchell A R and Covino J 1997 *Challenges in Propellants and Combustion 100 Years After Nobel* (New York: Begell House) p. 719

[3] Simonenko V N and Zarko V E 1999 "Comparative Study of the Combustion Behavior of Composite Propellants Containing Ultra Fine Aluminum", *Energetic Materials: 30th Int. Ann. Conf. ICT*, Karlsruhe, Germany, 1999, Vol. **21**, pp. 1–14

[4] Bashung B, Grune D, Licht H H and Samirant M 2000 "Combustion Phenomena of a Solid Propellant Based on Aluminum Powder", *5th Int. Symposium on Special Topics in Chemical Propulsion*, Stresa, Italy, 2000, Vol. **6**, pp. 19–22

[5] Mench M M, Kuo K K, Yeh C L and Lu Y C 1998 *Comb. Sci. Tech.* **135** 269

[6] Tulis A J, Sumida W K, Dillon J, Comeyne W and Heberlein D C 1998 *Arch. Comb.* **18** 157

[7] Lefran A A and Gallic C L 2001 "Expertise of Nanometric Aluminum Powder on the Detonation Efficiency of Explosives", *32nd Int. Ann. Conf. ICT*, Karlsruhe, Germany, 2001, Vol. **7**, pp. 3–6

[8] Dorsett H E, Brousseau P and Cliff M D 2001 "The Influence of Ultrafine Aluminium upon Explosives Detonation", *28th Int. Pyrotechnics Seminar*, Adelaide, Australia, 2001, Vol. **11**, pp. 4–9

[9] Gao D L, Zhang W, Zhu H and Liu X C 2007 *Journal of Solid Rocket Technology* **30** 420

[10] Lee K N and Worrell W L 1989 *Oxid. Met.* **32** 357

[11] Lee K N and Worrell W L 1994 *Oxid. Met.* **41** 37

[12] Zhang J J and Zhang H 2010 *Acta Phys. Sin.* **59** 4143 (in Chinese)

[13] Hohenberg P and Kohn W 1964 *Phys. Rev.* **13** 864

[14] Kohn W and Sham L J 1965 *Phys. Rev.* **140** 1133

[15] Clark S J, Segall M D, Pickard C J, Hasnip P J, Probert M J, Refson K and Payne M C 2005 *Zeitschrift Fur Kristallographie* **220** 567

[16] Perdew J P, Burke K and Ernzerhof M 1996 *Phys. Rev. Lett.* **77** 3865

[17] Wang M M, Ning H, Tao X M and Tan M Q 2011 *Acta Phys. Sin.* **60** 047301 (in Chinese)

[18] Simonovic D and Sluiter M H F 2009 *Phys. Rev.* B **79** 54304

[19] Scheffler M and Stampfl C 2000 "Theory of Adsorption on Metal Substrates", in: K. Horn and M. Scheffler (eds.), *Handbook of Surface Science*, Vol. **2** *Electronic Structure*, (Amsterdam: Elsevier) pp. 286–357

[20] Chakraborty B and Siegel R W 1983 *Phys. Rev.* B **27** 4535

[21] Kittel C 1996 *Introduction to Solid State Physics* 7th edn. (New York: Wiley)

[22] Pawluk T, Hirata Y and Wang L C 2005 *J. Phys. Chem.* B **109** 20817

[23] Juarez L F, Da S, Stampfl C and Scheffler M 2005 *Phys. Rev.* B **72** 075424

[24] Zhukovskii Yu F, Jacobs P W M and Causá M 2003 *J. Phys. Chem. Soilds* **64** 1317

[25] Zhang H, Soon A, Delley B and Ctampfl S 2008 *Appl. Surf. Sci.* **254** 7655

[26] Zhang H and Li W X 2009 *J. Phys. Chem.* C **113** 21361

[27] He Y B, Stierle A, Li W X, Farkas A, Kasper N and Over H 2008 *J. Phys. Chem.* C **112** 11946

[28] Chan C M, Cunningham S L, van Hove M A, Weinberg W H and Withrow S P 1977 *Surf. Sci.* **66** 394

[29] Juarez L F, Da S and Catherine S 2008 *Phys. Rev.* B **77** 045401

[30] Xu G X and Wang X Y 2010 *The Structure of Matter* (Beijing: Science Press) p. 94